Importance of Mass Transport and Spatially Heterogeneous Flux Processes for In-Situ Atomic Force Microscopy Measurements of Crystal Growth and Dissolution Kinetics

*Massimo Peruffo,[†] Michael M. Mbogoro,[#] Maria Adobes-Vidal and Patrick R. Unwin**

Electrochemistry and Interfaces Group, Department of Chemistry, University of Warwick, Coventry, CV4 7AL

[*] To whom correspondence should be addressed: Tel: (+44) (0)24 7652 3264
Email: p.r.unwin@warwick.ac.uk

† Present address: Johnson Matthey Fuel Cells, Lydiard Fields, Great Western Way, Swindon, SN5 8AT, United Kingdom. Email: Massimo.peruffo@matthey.com

Present address: Isis Innovation Ltd. Buxton Court, 3 West Way, Oxford, OX2 0SZ, United Kingdom. Email: Michael.Mbogoro@innovation.ox.ac.uk

ABSTRACT

It is well-established that important information about the dissolution and growth of crystals can be obtained by the investigation of step movement on single crystal faces via in-situ AFM. However, a potential drawback of this approach for kinetic measurements is that the small region of investigation may not be representative of the overall surface. It is shown that the investigation of local processes without accounting for the processes outside the region of interest can lead to significant misinterpretation of the data collected. Taking the case of gypsum dissolution as an exemplar, we critically analyze literature data and develop 3 different finite element method models that treat in detail the coupled mass transport – surface kinetic problem pertaining to dissolution processes in typical AFM environment. It is shown that mass transport cannot be neglected when performing *in-situ* AFM on macroscopic surfaces even with high-convection fluid cells. Moreover, crystal dissolution kinetics determined by AFM are mainly influenced by processes occurring in areas of the surface outside the region of interest. When this is recognized, and appropriate models are applied, step velocities due to dissolution are consistent with expectations based on macroscopic measurements and the kinetic gap that is often apparent between nanoscale and macroscopic measurements is closed. This study provides a framework for the detailed analysis of AFM kinetic data that has wide utility and applicability.

INTRODUCTION

The measurement and interpretation of mineral (or, more generally, crystal) dissolution and growth kinetics is important in many areas of chemistry, as well as in the allied fields of geochemistry and materials science.[1,2] Such processes generally involve mass transport coupled to interfacial processes, and the reliable elucidation of dissolution and growth kinetics requires a clear demarcation of mass transport, on the one hand, and surface (interfacial) kinetic components, on the other.[3-5] Moreover, studies are most informative when the focus is well-defined (single crystal) surfaces.[3,4]

Increasing attention focuses on local dissolution behavior, using high-resolution techniques such as atomic force microscopy (AFM).[6-18] In these studies, the dissolution process is investigated through the evolution of the crystal surface morphology at a microscopic/molecular level, and kinetics are often deduced from the analysis of the surface retreat.[7,11,15,16,18] In many cases, the main mode of dissolution is by step motion, and the step position is tracked over time to determine step velocities, from which dissolution kinetics have been determined.[19,20]

In-situ AFM has been particularly lauded for its capacity to capture high resolution images of dynamic processes on surfaces at the nanoscale/microscale.[8,10-14,21-25] On the other hand, it is also recognized that this technique is typically limited to slow processes or to reactions that are only accessible at low driving force (close to equilibrium conditions) because changes in the surface topography must be slower than the image acquisition rate.[19] An exception is integrated electrochemical (IE)-AFM,[6,26] or equivalently combined scanning electrochemical microscopy (SECM)-AFM, which allow the solution conditions to be changed rapidly and significantly, while changes in the substrate are mapped as the process comes back to equilibrium.[27-29] Such studies are relatively rare.

Most contemporary investigations have coupled AFM to a fluid cell to: (i) replenish bulk media, so as to counteract the accumulation of dissolution products; and (ii) supposedly render complications due to mass-transport negligible, by flowing solution at rates sufficiently high for observed step velocities to remain constant with increasing flow rate.[9,19,20,30-37] The attainment of this condition is taken to be diagnostic of a surface-controlled reaction. However, the hydrodynamic behavior in such fluid cells is known to be complicated,[38] and an alternative interpretation could be that although convection rates change, mass transport in the region of the AFM measurement (which depends on convection and diffusion) is largely unaffected. This would naturally lead to a misinterpretation of the kinetic regime, and is one of the issues that we explore in this paper.

There are other examples where there is a significant mismatch in nanoscale/microscale kinetic measurements, determined via AFM, and macroscopic kinetics.[20,35-37] Moreover, and perhaps of greater concern, is that for some crystal materials (*vide infra*), AFM dissolution studies conducted under apparently similar experimental conditions (undersaturation, flow rates, etc.) yield widely divergent values for step velocities and, consequently, the reaction rates that are extracted. The reasons for these significant discrepancies have not yet been sufficiently well explained and so, in this paper, we address key issues for *in-situ* AFM by critically analyzing local dissolution data for a ubiquitous mineral aqueous system, namely gypsum ($CaSO_4 \cdot 2H_2O$). Significantly, we identify some common misconceptions that have arisen in the *in-situ* AFM dissolution (growth) literature and identify the likely origin of discrepancies between dissolution studies conducted under similar conditions.

Gypsum is a common sedimentary mineral, of major interest in geochemistry[39] and with applications in the construction industry.[40] Traditional studies on gypsum dissolution kinetics

have been summarized[41] in a review that sought to rationalize and explain the impact of different experimental set ups, especially mass-transport conditions, on measured macroscopic dissolution rates. Yet, there is not yet a general consensus from local studies. For example, several works[42-45] have reported step velocity values for dissolution from steps with the same orientation on the basal (010) plane of gypsum, which vary by a factor of ≈ 10, for apparently similar experimental conditions. Furthermore, as we highlight herein, local dissolution rates do not match macroscopic dissolution rates; local rates are typically lower by one to two orders of magnitude (*vide infra*).

We note that the importance of mass transport in AFM fluid cells for the case of arrays of microcrystals was treated in detail via a finite element method analysis, for the particular case of calcium oxalate monohydrate (COM) crystal growth.[38] For this system, the AFM wafer, cantilever and tip were shown to block diffusion to microcrystals in their vicinity under typical flow conditions, but because COM is characterized by slow interfacial kinetics, tip perturbations were rather small. It was, however, pointed out that inorganic materials with faster interfacial growth kinetics could be impacted more significantly. This paper considers such a case of faster (dissolution) kinetics, but also a configuration with much larger crystals which are studied most widely by *in-situ* AFM.[12,15,18,19,31,35,45,46] We show that both aspects –faster kinetics and larger crystals– significantly complicate local mass transport and interfacial fluxes, with significant implications for the quantitative analysis of AFM dissolution (and, by extension, crystal growth) data.

EXPERIMENTAL

To inform the modeling that follows, we carried out crystal etching studies were designed to mimic the experimental conditions used in prior work considered herein, and to identify the types of features and step density which are produced. Gypsum was obtained as natural optically clear selenite (St-Gobain Gyproc). Fresh surfaces were prepared by careful cleavage along the (010) plane with a sharp scalpel. These were treated with a strong short burst of N_2 gas (BOC) to yield pristine flat surfaces devoid of large macrosteps and adhered micro-fragments. Using tweezers, a freshly cleaved sample was secured onto a sample holder with the surface of interest flush against the etching solution of ≈ 250 ml volume. This was either ultrapure Milli-Q reagent grade water (Millipore) with a typical resistivity of 18.2 MΩ cm (25 ^{o}C) or 6.4 mM $CaSO_4$ (Sigma-Aldrich, calcium sulfate dehydrate ACS reagent > 99%) aqueous solution made up in Milli-Q water, giving a relative saturation level of $\Omega = C^{sat}/C = 0.4$ (*vide infra*). Gentle stirring was applied using a magnetic flea. Experiments were run for ≈ 60 min, after which the samples were immediately dried under N_2 gas, and surfaces analyzed via optical differential interference contrast (DIC) microscopy (Leica DM 4000M).

THEORY AND MODELING

Numerical simulations were performed on a Dell Intel i7 3.40 GHz computer equipped with 32 GB RAM running Windows 7 Enterprise 64 bit edition. All simulations were performed using the commercial finite element modeling package COMSOL Multiphysics 4.3a (COMSOL AB, Sweden). 2-D and 3-D simulations were performed using triangular and tetrahedral mesh elements, respectively. For each geometry, the mesh density was optimized by decreasing the mesh size until no detectable difference was evident in the simulation results with finer mesh

density. The mesh density was highest close to sharp edges and at the boundaries where flux conditions were applied, leading to (steep) concentration gradients.

Mass transport-kinetic models for the dissolution of a crystal surface by step retreat were developed. This enabled step velocities to be predicted for a range of intrinsic dissolution rates applied at the crystal surface, with the possibility of mass transport (diffusion) limitation between the crystal surface and solution. Figure 1**a, b** shows a cartoon of the model geometries (not to scale), where letter labels define particular boundaries, whose size is reported in Table 1, and the numbers are used to define the boundary conditions applied (*vide infra*).

In Figure 1**a**, we consider the simplest uniform step (US) model, in which an array of steps from which dissolution occurs, is evenly distributed with a constant periodicity across an essentially infinite substrate. This was created using a domain representing a repeat unit of a single step on a planar surface, where A_{sd} defines the step density. This was varied in the simulations so that a range of step densities were considered. H_b defines the thickness of the concentration boundary layer (CBL), which is controlled by the hydrodynamic regime, such that bulk composition prevails at boundary **2**, and H_{step} is the step height. A second 2-D model, which we term the outer flux (OF) model, Figure 1**b** (not to scale), describes a more realistic situation in which there is a region of interest (ROI) with uniform step distribution, surrounded by an outer area of different activity (A_a). The ROI defines the portion of the crystal surface that would be targeted by the *in-situ* AFM, while the area beyond this may have different activity. To ensure that we do not over-emphasize the impact of this area we have inserted an inactive buffer area (A_i) between the two. This serves to reduce the impact of the outer active area and so our results should be seen as conservative in terms of the influence of reactions outside the ROI on the ROI itself. Based on surface topography data presented later, these are reasonable 2D diffusion

models. We ignore the tip, which might be expected to further impact mass transport,[38,47] and so are presenting the case of the maximum mass transport rates possible. Our results thus represent a lower bound to the influence that mass transport will have on surface kinetics.

The domain of a further model, which simulates an AFM fluid cell, is shown in Figure 1**c, d**, using the geometry based on the MTFML AFM fluid cell (Bruker). This 3D model investigates the influence of convection and the impact of the AFM tip/holder and general cell geometry on mass transport in a square ROI for a setup in which the bottom wall of the AFM fluid is formed by the crystal surface under investigation, as in a number of studies.[12,15,18,19,31,35,44,45] The surface concentration at the ROI is simulated at different flow rates and for different bulk concentrations.

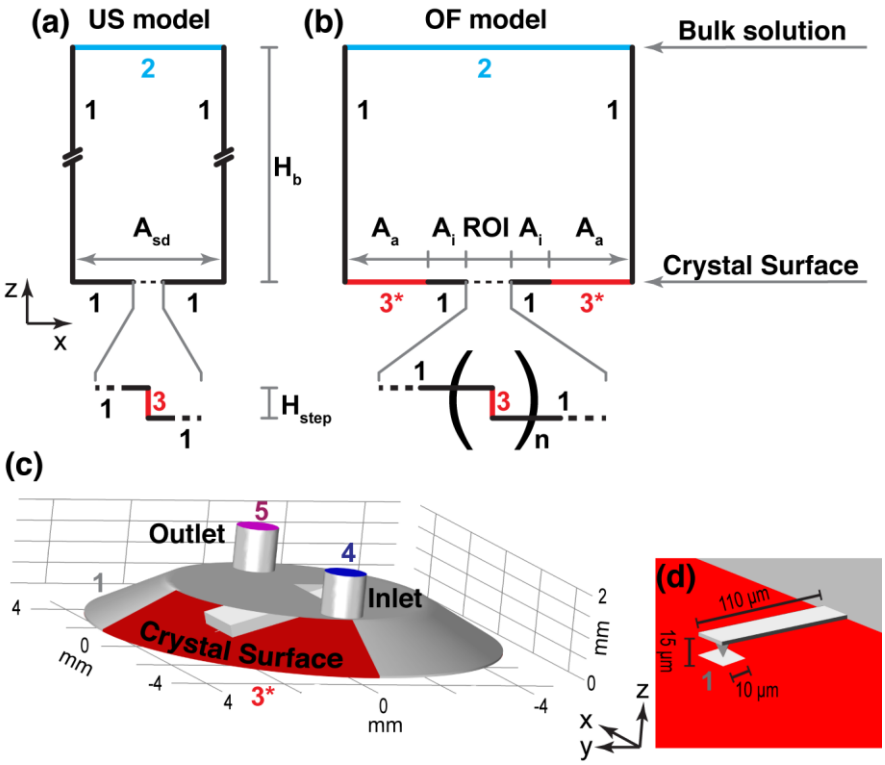

Figure 1. 2D representations of: (a) the US model, with uniformly distributed steps on an infinite surface (A_{sd}); and (b) the OF model with an area of uniformly distributed steps (ROI) surrounded by a non-active area (A_i), which, in turn, is surrounded by an active region that represents

average macroscopic surface (A_a). (c) AFM flow cell model. The letters represent geometric dimensions and numbers the boundaries conditions applied to numerical simulations.

Dissolution of an ionic crystal is a stoichiometric reaction to satisfy the assumption of an electro-neutral solution and to maintain a constant charge at the crystal surface; as such, for illustrative purposes we reduce the mass transport model to the simulation of a single species. Calcium and sulfate ions (and the ion pair) can reasonably be considered to have similar diffusion coefficients (D) and it was appropriate to use the average, $D = 0.9 \times 10^{-9}$ m^2 s^{-1}.[48] Seeking to identify general trends that could be applied to related systems, the model deliberately ignored speciation and ion pairing effects, which would not be expected to impact significantly.[49] The solubility (C^{sat}) of gypsum, as the total amount of calcium/sulfate dissolved at equilibrium, was calculated to be 16.2 mM in pure H_2O using the numerical code MINEQL+ (Environmental Research Software, version 4.5),[50] in agreement with experimental measurements.[41]

Table 1. Parameter ranges and values applied to the numerical simulations. Model geometries and labels defined in Figure 1

Boundary	Size		
A_{sd}	0.01–10 μm (100 – 1 μm^{-1})	C^{sat}	16.2 mM
ROI	10 μm	C_b	0, 6.4, 8, 12 mM
A_i	1 – 10 μm	V_f	1, 5, 10, 50 μl s^{-1}
A_a	20 μm	D	0.9 ×10^{-9} m^2 s^{-1}
H_{step}	1 nm	k_{step}^{intr}	1 ×10^{-6} – 5 ×10^{-4} m s^{-1}
H_b	200 μm	k^{app}	1 ×10^{-6} – 7.5 ×10^{-5} m s^{-1}
N	10, 40 (d_{step} = 1, 4 μm^{-1})	MV	13400 mol m^{-3}

The boundary condition applied to the numerical models, as defined in Figure 1, are as follows: the vertical external walls of the diffusion cell, the 'inactive' parts of the basal crystal surface and the AFM fluid cell walls, i.e. all boundaries numbered **1** in each of the parts in Figure 1, are inert and a zero normal flux boundary condition was applied

$$\mathbf{n} \cdot (D \nabla C) = 0 \qquad (1)$$

where **n** is inward pointing unit vector normal to the boundary and C is the concentration of the calcium and sulfate ions.

Due to forced convection in AFM fluid cells, we can reasonably consider a well-defined CBL[51] for the US and OF models. The top boundary (numbered **2**) thus defines a limit beyond which the solution can reasonably be considered to attain the bulk condition:

$$C = C_b \tag{2}$$

where C_b is the bulk concentration of the calcium and sulfate ions. Boundaries **3** and **3*** define steps on the surface and the uniformly active outer surface region (A_a), respectively. A flux condition was applied on these boundaries

$$\mathbf{n} \cdot (D\nabla C) = \boldsymbol{J}_\perp \tag{3}$$

where $\boldsymbol{J}_\perp$ is the inward normal flux of dissolving species. Dissolution of gypsum under highly undersaturated conditions is often described by a first-order reaction[52,53] and the normal flux magnitude at these surfaces is consequently reasonably defined by:

$$\boldsymbol{J}_\perp = k^i (C^{sat} - C) \tag{4}$$

where k^i is a surface rate constant, with units of m s^{-1}. For boundary **3** we use the terminology i = intr, and the rate constant (k_{step}^{intr}) is the intrinsic dissolution rate constant at the step. For boundary **3*** we use the terminology i = app and the rate constant (k^{app}) defines a rate coefficient for an apparent rate law applied to the active areas, using the approximation of a uniformly active surface. This is reasonable, as the idea of this zone is to represent the general kinetic characteristic of the crystal dissolution process, and in this area the CBL is orders of magnitude larger than any surface heterogeneity. Obviously, our model could be developed to be applied to many kinetic situations, but a first-order process is perfectly adequate for illustrative purposes.

The velocity of a step, u_{step}, can be calculated from the magnitude of the inward flux normal to a step ($J_\perp$):

$$u_{\text{step}} = J_{\perp} \big/ MV \tag{5}$$

where MV is the molar volume of gypsum.[54] For both the US and OF models, the velocity of the steps was calculated from the simulation results as the average of the normal flux at the steps (boundary **3**). Note that for the OF model, where the active area outside the ROI typically has a higher flux, there is a decrease of the normal flux at steps towards the edge of the ROI, but, to a first approximation, the velocity is calculated from the average of the normal flux at all steps in the ROI.

For the US and OF models, the mass transport of material in the domains of interest is described by a steady-state diffusion equation:

$$D\nabla^2 C = 0 \tag{6}$$

Furthermore, we apply a static model, by reasonably assuming a relatively low step velocity with respect the characteristic diffusion time, $t_{\text{diff}} = l_{\text{p}}^2 / D$, where l_{p} is the characteristic length of interest, which – in this case – is the height of the step investigated (H_{step}). This assumption is easily satisfied for all cases investigated. Moreover, for closely spaced steps, and relatively high fluxes (typical of the gypsum system), there is diffusional overlap of dissolved material from individual steps, after a short distance from the surface (*vide infra*), so that the whole surface may be considered to behave as an essentially uniformly active surface in the areas A_{sd} (US model), ROI (OF model) and the overall crystal surface in the AFM fluid cell model (*vide infra*). This, of course, is a further justification for applying a uniform flux to boundary **3*** when

investigating the impact, on the ROI, of processes that occur outside this area for the OF model and the fluid cell simulations.

For the AFM fluid cell model (Figure 1**c**), steady-state convective-diffusion mass transport applies, as described by:

$$D\nabla^2 C - \mathbf{v} \cdot \nabla C = 0 \tag{7}$$

where v (with components v_1, v_2 and v_3, in the x, y and z directions, respectively) is the velocity vector solved using incompressible Navier-Stokes equations for momentum balance (eq 8) and continuity (eq 9)

$$\rho \mathbf{v} \cdot \nabla \mathbf{v} = -\nabla p + \eta \nabla^2 \mathbf{v} \tag{8}$$

$$\rho \nabla \mathbf{v} = 0 \tag{9}$$

where ρ is the density of the solution (1.00 g cm^{-3} was used, as for pure water), η is the dynamic viscosity, assumed to be 1.00 mPa s[55] and p is the pressure.

For the calculation of fluid flow, the following boundary condition was applied on boundaries **1** and **3**

$$\mathbf{v} = 0 \tag{10}$$

Boundary **4** is an inlet tube, where it is reasonable to apply a flux defined by fully developed laminar flow, with flow rate, V_f, down a tube of radius, r_0, with r the radial co-ordinate with respect to the tube axis:

$$v_r = \frac{V_f}{\pi r_0^2}\left(1 - \frac{r^2}{r_0^2}\right) \tag{11}$$

For boundary **5**:

$$p = 0, \mathbf{n} \cdot \eta \nabla^2 \mathbf{v} = 0 \tag{12}$$

The boundary conditions applied to solve convective-diffusion mass transport in the AFM cell are as follow. For boundaries **1** and **3***, eq 1 and eq 3 apply, respectively. Boundary **4** is defined by eq 2 and at boundary **5** it is reasonable to apply an outflow in which convection is the dominant mode of mass transport:

$$-\mathbf{n} \cdot (D \nabla C) = 0 \tag{13}$$

RESULTS AND DISCUSION

Mass transport and kinetics: Analysis of AFM and macroscale measurements

We begin with an overview of previous kinetic measurements, to provide a rationale for the analysis that follows. The plot in Figure 2 summarizes the step velocities ([100]-oriented and [001]-oriented steps) at different undersaturation conditions deduced for a number of *in-situ* AFM gypsum dissolution studies of the (010) basal surface. Table 2 further presents the corresponding dissolution rates extrapolated from step velocities for some of the studies performed under similar conditions of saturation, where the step density ($d_{step} \approx 1\ \mu m^{-1}$) and step height ($H_{step} \approx 0.8$ nm) can be estimated from the images presented in the works referred. In deducing these fluxes, only the [100]-oriented steps were considered, as this step moves at least an order of magnitude faster than the [001]-oriented steps[43] and is just as abundant on the surface and so contributes overwhelmingly to the dissolution flux. The gross dissolution rates calculated over the geometric surface (G_{surf}) were thus estimated from:

$$G_{surf} = u_{step} \cdot MV \cdot H_{step} \cdot d_{step} \qquad (14)$$

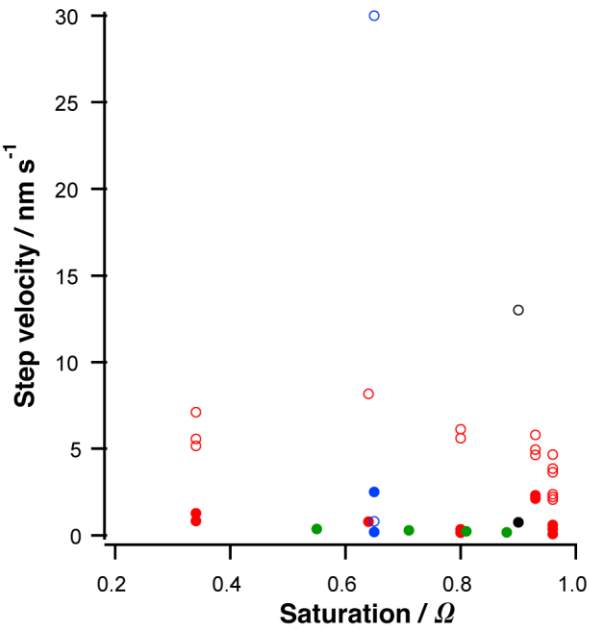

Figure 2. Gypsum step velocities at different saturations for [001] (empty circles) and [100] (solid circles) oriented steps. Data are from the literature, with the following references: red,[44] blue,[43] green[45] and black.[32]

The data in Figure 2 and Table 2 clearly demonstrate how the step displacement velocities measured via *in-situ* AFM experiments, for dissolution studies under similar experimental conditions (saturation level), typically span at least an order of magnitude. Moreover, there is no sensible relationship of the step velocity (dissolution kinetics) with saturation level (Figure 2). This is even true within individual studies. For example, It was found that [100]-oriented steps had a constant velocity ≈ 7 nm s^{-1} for a wide range of saturation ($\Omega = C^{sat}/C = 0.3 - 0.9$),[30] which is not consistent with basic kinetic laws in which higher driving force (low saturation) would expected to correspond to a faster dissolution rate (faster step velocity). It has been proposed that heterogeneity of flux (local dissolution rate) at different areas of a crystal surface would impact AFM dissolution studies,[19] but there was no further analysis. A decrease of observed step

velocity in areas of the surface with higher step density was also noticed in some studies.[20] As we demonstrate herein, this observation clearly indicates a strong influence of mass transport on the step velocity (see results of the US model below). A further study reported a decrease of step velocity in regions of the surface close to (active) etch pits,[43] but did not rationalize this observation. Again, this is clear sign of the significant influence of a neighboring reactive flux on the movement of steps in a ROI, as we show herein for the OF model.

Table 2. [100]-oriented step velocities and related gross dissolution rates calculated for $d_{step} \approx 1\ \mu m^{-1}$ and $H_{step} \approx 0.8$ nm

Ω	u_{step} / nm s^{-1}	G_{surf} / mol m^{-2} s^{-1}	Reference
0.65	≈ 30	3.2×10^{-7}	[43]
0.80	≈ 13	1.4×10^{-7}	[32]
0.90	≈ 5	5.4×10^{-8}	[45]
0.96	≈ 2	2.1×10^{-8}	[44]

One of the most notable features of Table 2 is that the dissolution rates extrapolated from step velocities, from *in-situ* AFM experiments, are always much smaller than fluxes from macroscopic dissolution experiments by several orders of magnitude (*vide infra*). A similar situation has been found in other systems, such as calcite dissolution, where the local dissolution rate calculated from step velocity is much lower than gross dissolution rates, even when measured in the same setup.[35,37] The analysis that we develop herein serves to rationalize and explain this behavior.

The macroscopic dissolution of gypsum is reported to be mass transport controlled or under mixed-kinetic control depending on the forced convection set-up used and mass transport rates generated.[41] Although forced convection provides access to higher transport rates, a number of studies using the rotating disk (RD)[56,57] and high flow rate channel flow cell (CFC)[49] measured the G_{surf} in the range 1×10^{-5} - 5×10^{-5} mol m^{-2} s^{-1} for a variety of Ω and hydrodynamic conditions, proving that gypsum dissolution remains under mixed-kinetic control even in hydrodynamic systems.[41] For experiments conducted under a range of well-defined mass transport regimes, an extrapolation is possible to estimate the intrinsic gross dissolution rate which was found to be $G_{surf}^{intr} = 5 \pm 2 \times 10^{-5}$ mol m^{-2} s^{-1} for the (010) surface.[41] This is at least two orders of magnitude higher than the rates extracted from step velocity measurements via *in-situ* AFM (Table 2). This is a significant difference given that the surfaces in the macroscopic studies and AFM measurements are the same and the rates deduced from AFM and macroscale measurements can supposedly be compared free from mass transport effects. Interestingly, etch pit studies from our group have confirmed the intrinsic kinetic constant for the recession of the (010) surface during dissolution, but have measured step velocities, free from mass transport limitations, which are several orders of magnitude larger than deduced by AFM.[58] The question thus arises as to whether the AFM measurements are simply not representative of the major processes or whether there are more significant limitations?

Under purely mass transport control, or mixed-kinetic conditions (i.e. limitations from mass transport and surface kinetics), a CBL is formed, where the concentration at the surface differs from the bulk concentration ($C_{surf} > C_b$), so that to obtain intrinsic dissolution kinetics C_{surf} must to be known. The hydrodynamics of an AFM fluid cell, for the situation in which the bottom surface of the AFM cell is the dissolving crystal surface, can reasonably be approximated by an

open channel cell (OCC).[33] The solution sweeping over the dissolving surface accumulates material, leading to an increase of the CBL thickness along the direction of the flow stream lines. The CBL thickness is function of the geometry of the cell and the flow rate and it can be as large as 1 - 3 mm.[33] Hydrodynamic modeling in this paper indicates a value of 200 µm (*vide infra*) for an AFM fluid cell of a volume of ≈ 100 µl and flow rate (V_f) of 100 µl s^{-1}. This flow rate is high for such a cell and thus represents the practical upper limit on the mass transport rates that can be generated.[38] The comparison between the transport rate constant $k^t = D / \delta = 4.5 \times 10^{-6}$ m s^{-1} for δ = 200 µm (the maximum mass–transport rate possible) and the experimental value of $k_{surf}^{intr} = 6 \pm 1.5 \times 10^{-6}$ m s^{-1} [41] clearly shows that mass transport can never be neglected in such a cell./In fact, that there will always be strong mass transport effects for AFM dissolution studies of gypsum, especially as the tip would further inhibit local mass transport[38] (decreasing k^t).

It is also important to point out that one should not confuse the cell solution residence time or "washout time" with interfacial mass transport rates. For example, for a flow rate of 100 µl s^{-1}, the washout time for the AFM fluid cell described above is rather quick at 1 s. This is enough to avoid significant accumulation of material within the cell, but not to prevent the formation of an extensive CBL.

Surface topography pertaining to AFM studies

In-situ AFM studies of crystal dissolution commonly require some time to optimize the conditions for high quality imaging, and the actual experiments could typically take a few hours in practice. During this time, the crystal is in contact with the etching medium and the surface undergoes the dissolution process. Crystal dissolution on a macroscopic cleaved crystal surface is often initiated by the nucleation of pits at active sites, i.e. point/line defects and

dislocations.[59,60] Further dissolution of pits, and the spreading of steps originating at pits or defects leads to a surface with an activity and morphology that evolves continuously, but is spatially heterogeneous,[61] depending on the length scale, as depicted in Figure 3**a, b, c.** These are typical optical DIC images of gypsum ((010) plane) after etching for 60 min in: (**a, b**) pure water; and (**c**) a bulk saturation level, $\Omega \approx 0.4$ (6.4 mM $CaSO_4$). The surface is characterized by a generally high step density, but this is heterogeneous across the surface. Small areas, clear of macro-step features can be found, e.g. the yellow circles in Figure 3**a, b, c**. AFM experiments would commonly be performed in such areas (usually square areas of 10 - 20 μm length constituting the ROI) to measure the displacement of monoatomic steps, from which dissolution kinetics are derived.[32,33,43-45] On the other hand, it can be seen that neighboring these apparently flat areas are regions with very high step density. We show below, in the context of the OF model, that such features may impact significantly on the step velocity measured in the ROI. The general situation is highlighted in Figure 3**d**: a small ROI is selected for AFM studies, but significant activity outside the ROI could be expected to impact the ROI itself. It can be seen that parallel steps are the dominant surface features on the gypsum (010) surface, allowing a 1-D representation of the crystal surface, and hence 2D diffusion equation, for both the US and OF models (Figure 1).

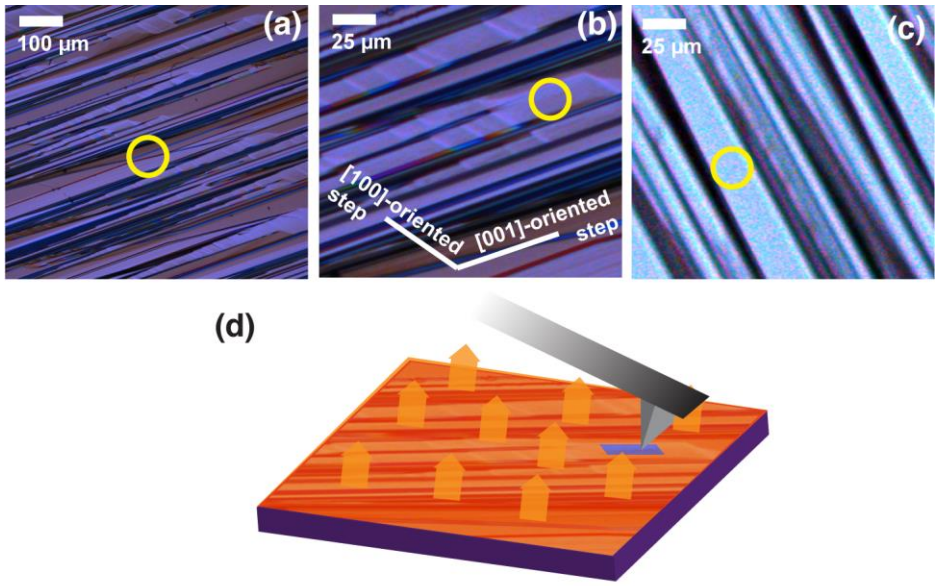

Figure 3. (**a**, **b**) Optical DIC image of a gypsum (010) cleaved surface after etching for 60 min in pure water and (**c**) in 6.4 mM $CaSO_4$. (**d**) Schematic representation of a typical *in-situ* AFM scan area on a macroscopic surface where there is a dissolution flux from the active surface surrounding the scanned area.

Uniform step (US) model

The US model (Figure 1**a**) considers a uniform step density to be entirely representative of the whole surface. For specified dissolution kinetics, the model elucidates the influence of the step density on the step velocity and enables the calculation of the gross dissolution rate (G_{surf}) for a range of step density comparable to that seen in previous AFM measurements.[43, 54-56] We considered values of $k_{step}^{intr} = 1 \times 10^{-6} - 5 \times 10^{-4}$ m s^{-1} as the step surface boundary condition, which covered a wide range of interest.[58]

As discussed above, the hydrodynamics of an AFM fluid cell can be approximated to an OCC for which a value of H_b = 200 µm is typical. Figure 4**a**, **b** reports the concentration profile

of the modelled domain (the step is located on x = 0, see Figure 4**a** inset) for a high intrinsic dissolution rate constant (k_{step}^{intr}) of 2.5 $\times 10^{-4}$ m s^{-1}, for 2 very different step densities of (**a**) 0.1 μm^{-1} and (**b**) 100 μm^{-1}. It is clear that at high step density, there is a significant accumulation of material at the crystal surface, as can reasonably be expected, due to the high density of active sites. Moreover, it can be seen that the pattern of mass transport for these cases is different (**a** vs **b**): there is a hemispherical diffusion field (Figure 4**a** inset) associated with diffusionally isolated steps, but significant interaction at close step spacing, so that a planar CBL develops (Figure 4**b**). Although, there is a higher gross dissolution rate with the higher step density, it is also important to point out that the step velocity decreases significantly with increasing step density for any k_{step}^{intr}, as shown in the 3-D plot in Figure 4**c**, which gives the step velocity as function of k_{step}^{intr} and step density. This highlights the important effect of step edge density on step movement for a defined step kinetic rate law.

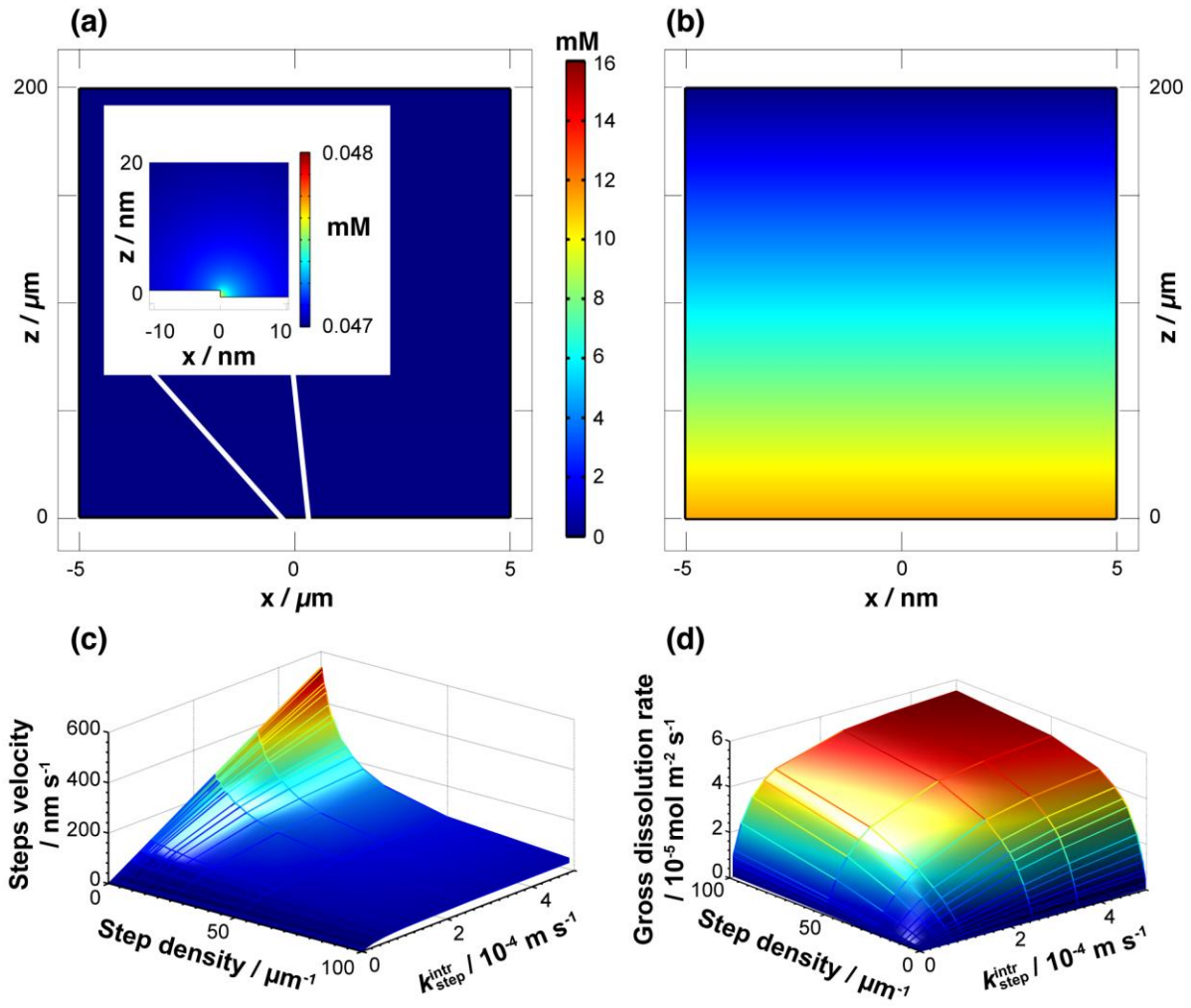

Figure 4. (**a**, **b**) Concentration profiles from the US models for k_{step}^{intr} = 2.5 ×10^{-4} m s^{-1}, C_b = 0 mM, H_{step} = 1 nm and d_{step}: (**a**) 0.1 μm^{-1} and (**b**) 100 μm^{-1}. (**c**) Step velocity as a function of step density and step intrinsic dissolution rate constant for C_b = 0 mM. (**d**) Gross dissolution rate as function of step density and step intrinsic dissolution rate for C_b = 0 mM. H_b = 200 μm.

From the plot in Figure 4**c**, at low step density d_{step} < 5 μm^{-1} (typical for the AFM studies reviewed herein, *vide supra*), the dissolution process is under strong surface kinetic control, however, from Figure 4**d** the gross dissolution rate is < 5 ×10^{-6} mol m^{-2} s^{-1}, which is an order of

magnitude lower than batch experiments.[41] This is true even for step velocities as high as 500 nm s^{-1} ($k_{step}^{intr} = 5 \times 10^{-4}$ m s^{-1}), which is orders of magnitude higher than measured by AFM (Figure 2). Significantly, for experimentally measured step velocities reported in Table 2 that are < 30 nm s^{-1}, the gross dissolution rate that results is < 4×10^{-7} mol m^{-2} s^{-1} for d_{step} < 5 μm^{-1}, a dissolution rate that is at least 2 order of magnitude lower than found from macroscopic measurements.

Thus, the US model highlights some key points pertaining to AFM dissolution studies. To observe the gross dissolution rates that have been determined via macroscopic techniques,[41] requires a much higher step velocity and / or density than ever encountered in AFM investigations. Moreover, as reported in Figure 4**d**, under such conditions, mass transport limitations prevail for the gypsum system,[41] which prevents the determination of surface kinetics.

Outer flux (OF) model

The OF model reflects more faithfully the situation of heterogeneous step density, that is seen in the topography of dissolved crystal faces, such as in Figure 3. The AFM scanned area (ROI) is represented by an area with well-defined and uniform step density, 1 to 4 μm^{-1}, typically in the range observed in AFM experiments,[32,44,45] surrounded by a high-density stepped zone (outer active area). As mentioned above, an additional inactive buffer area (varied in the range 1 - 10 μm) was introduced between the two regions. The rationale for this model is that, when the crystal surface is in contact with an etching medium, the gross dissolution rate measured for the same type of surfaces with macroscopic techniques has to be preserved. This is taken into account in the OF model, where an apparent dissolution rate constant (k^{app}) is applied to the active area outside the ROI. The step density in this area is high enough so that, as reported for this situation in the US model, the surface can be considered uniformly active.

The characteristic CBL thickness, for the OCC, was again set at H_b = 200 μm. Figure 5 reports the Ca^{2+} and SO_4^{2-} concentrations in the simulated domain for k_{step}^{intr} = 2.5 ×10^{-4} m s^{-1} (typical for [100]-oriented steps[58]) for the following cases: step density 1 μm^{-1}, (**a**) k^{app} = 0 and (**b**) k^{app} = 1 ×10^{-5} m s^{-1} (close to that for the basal (010) surface);[58] step density of 4 μm^{-1}, (**c**) k^{app} = 0 m s^{-1} and (**d**) k^{app} = 1 ×10^{-5} m s^{-1}. For cases (**a**) and (**c**), when the outer active area (A_a) is 'off' (inert) the concentration close to the steps is extremely low (< 0.3 mM), but increases with step density (compare **a** and **c**). The interfacial concentrations indicate that this is a strongly surface–controlled process (as found in the US model for this regime). However, when the active area is 'on' (**b** and **d**), the AFM ROI is flooded with dissolved material coming from the outer active area that accumulates at the crystal surface, and resulting in the formation a planar CBL. In fact, the concentration at the steps increases by 2 orders of magnitude (for a step density of 1 μm^{-1}) *purely due to processes outside the ROI*. The interfacial concentration of 10.5 mM, corresponding to a Ω = 0.65, is essentially set by *neighboring processes*.

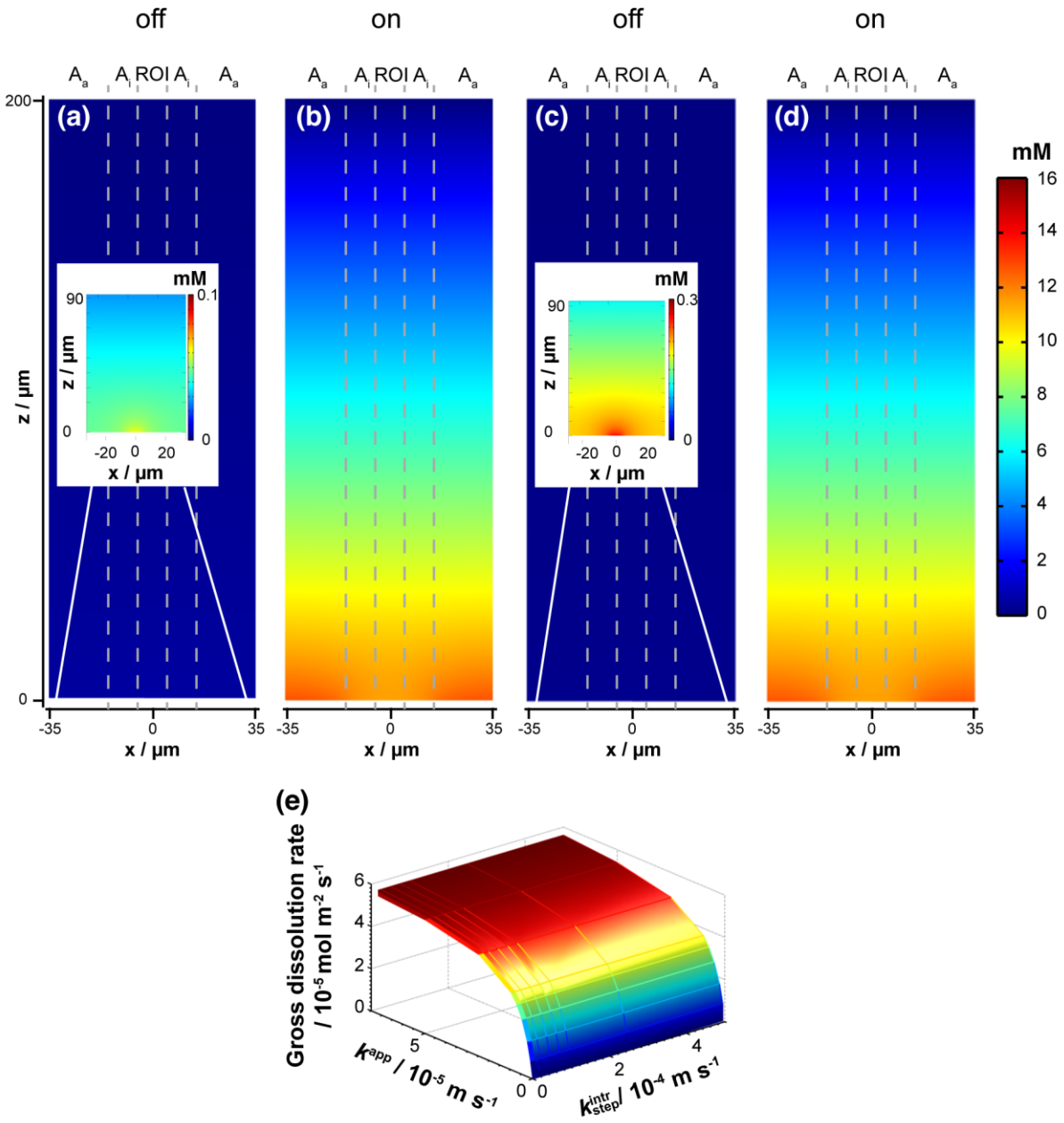

Figure 5. Concentration profiles for the OF model for k_{step}^{intr} = 1 ×10^{-4} m s^{-1}, H_{step} = 1 nm, C_b = 0 mM and A_i = 10 µm: (**a**) d_{step} = 1 µm^{-1} and k^{app} = 0; (**b**) d_{step} = 1 µm^{-1} and k^{app} = 1 ×10^{-5} m s^{-1}; (**c**) d_{step} = 4 µm^{-1} and k^{app} = 0; (**d**) d_{step} = 4 µm^{-1} and k^{app} = 1 ×10^{-5} m s^{-1}. Note that the steps located in the central area are not visible due to the vertical scale. (**e**) Gross dissolution rate (flux) as

function of intrinsic step dissolution rate constant and apparent dissolution rate constant in the outer active area for A_i = 10 μm, C_b = 0 mM and d_{step} = 1 μm^{-1}. H_b = 200 μm in all cases.

Figure 5**e** reports the gross dissolution rates as a function of k^{app} and k_{step}^{intr} for a step density of 1 μm^{-1}, which we have pointed out above, is typical of ROIs in AFM studies.[32,43-45] When the outer active area is switched 'off' (k^{app} = 0), the gross dissolution rate is extremely low < 10^{-6} mol m^{-2} s^{-1}, irrespective of k_{step}^{intr} over the range investigated, k_{step}^{intr} = 1 ×10^{-4} - 5 ×10^{-4} m s^{-1}. When the outer active area is 'on' the gross dissolution rate easily reaches a plateau close to 6 ×10^{-5} mol m^{-2} s^{-1} for k^{app} > 2 ×10^{-5} m s^{-1} and any value of k_{step}^{intr}. This is the mass-transport controlled situation but it is *dominated by the outer process*. This illustrates very clearly that one simply cannot investigate regions of a surface with low step density without accounting for what is happening elsewhere on the surface.

A clear appreciation of the impact of the outer active area comes when examining the step velocity as function of the intrinsic rate at step (k_{step}^{intr}) and the apparent dissolution rate constant at the active area (k^{app}). The data for a step density of 1 μm^{-1} and for 2 bulk concentrations, 0 and 6.4 mM (top to bottom), are plotted in Figure 6. There is a general trend in which the step velocity decreases steeply with an increase of k^{app} applied at the outer active area. For example, for case **b** the step velocity decreases from 158 nm s^{-1} to 56 nm s^{-1} for k_{step}^{intr} = 2.5 ×10^{-4} m s^{-1}, when k^{app} changes from 0 to 1 ×10^{-5} m s^{-1}. This clearly shows that the major influence on the dissolution reaction in the ROI is the process occurring in the outer active area.

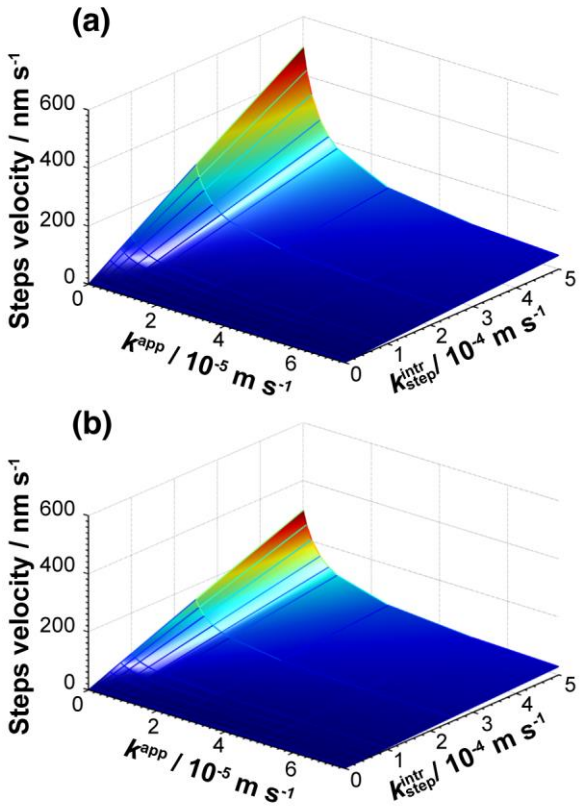

Figure 6. Step velocity as function of intrinsic step dissolution rate constant and apparent dissolution rate constant in the outer active area for d_{step} = 1 μm^{-1}, H_b = 200 μm, A_i = 1 μm and H_{step} = 1 nm with (**a**) C_b = 0 mM and (**b**) C_b = 6.4.

Table 3 lists the intrinsic rate constant (k_{step}^{intr}) for [100]- and [001]-oriented steps from past work, for 2 experimental cases, Ω = 0.65[43] and Ω = 0.80. The rate constants were calculated by rearranging eq 4 and eq 5 for a purely surface–controlled kinetic case, as assumed for *in-situ* AFM studies,[32,43] so that $C_{surf} = C_b$. The resulting values of k_{step}^{intr} are shown in the column headed 'Experimental AFM'. For comparison, the OF model was run using k_{step}^{intr} values that we recently measured from etching studies: k_{step}^{intr} = 2.5 ×10^{-4} m s^{-1} and 1 ×10^{-5} m s^{-1} for [100]-oriented step and [001]-oriented step, respectively,[58] from which the corresponding u_{step} was determined. In

the ROI we employed d_{step} = 1 μm^{-1}, as typical for AFM, with A_i = 1 μm. We used k^{app} = 1 ×10^{-5} m s^{-1} in the outer active area to ensure that the gross dissolution rate was consistent with macroscopic measurements. These data are reported in the column headed 'OF model'. Interestingly, the step velocities calculated (OF model) are seen to approximate very closely to the actual AFM experimental u_{step} values. However, the important point is that the kinetic constants used in the OF model calculation are at least an order of magnitude higher than one would conclude from AFM if one ignored the outer areas process as is commonly done. The data in Table 3 clearly highlight the danger of interpreting AFM ROI data without reference to processes outside, which modulate ROI steps velocities.

Table 3. Intrinsic rate constants from literature AFM step velocities, considering surface-controlled kinetics, compared with step velocities obtained using the OF model (d_{step} = 1 μm^{-1}, A_i = 1 μm, k_{app} = 1 ×10^{-5} m s^{-1}) with step velocities from optical microscopy etching studies[58]

Ω	Step orientation	Experimental		OF model	
		u_{step} / nm s^{-1}	k_{step}^{intr} / m s^{-1}	k_{step}^{intr} / m s^{-1}	u_{step} / nm s^{-1}
0.65[43]	[100]	≈ 30	6.8 ×10^{-5}	2.5 ×10^{-4}	≈ 30
	[001]	≈ 2.5	5.7 ×10^{-6}	1 ×10^{-5}	≈ 1.4
0.80[32]	[100]	≈ 13	5 ×10^{-5}	2.5 ×10^{-4}	≈ 16
	[001]	≈ 0.7	2.9 ×10^{-6}	1 ×10^{-5}	≈ 0.8

Our model allows us to explain other data in literature. For example, the extremely low step velocities that have been measured in one study[45] can be attributed to the low flow rate used (5 μl s^{-1}) that leads to a mass transport controlled situation (on average), *i.e.* the step velocity in the ROI is low because the interfacial concentration is close to saturated levels (retarding dissolution). A similar scenario is likely to apply to other results[44] where the kinetics did not follow any expected rate law, *i.e.* the step velocity did not change with the bulk saturation. Again, the low flow rate used (8 μl s^{-1}) leads to an accumulation of material at the crystal surface so that changing C_b simply does not significantly affect the interfacial concentration and consequently the dissolution rate (within experimental error). These mass–transport aspects are considered in more detail in the next section.

AFM fluid cell hydrodynamic model

Figure 7 shows the rather complex hydrodynamics in the AFM fluid cell, calculated using the model defined in the Theory and Modeling section,, for a volume flow rate of V_f = 50 μl s^{-1}. Note that the tip holder and the tip itself induce a substantial decrease of the local velocity of the flowing solution along the bottom surface of the AFM fluid cell. The decrease of convection close to the ROI naturally leads to a decrease in the mass transport rate in this region.

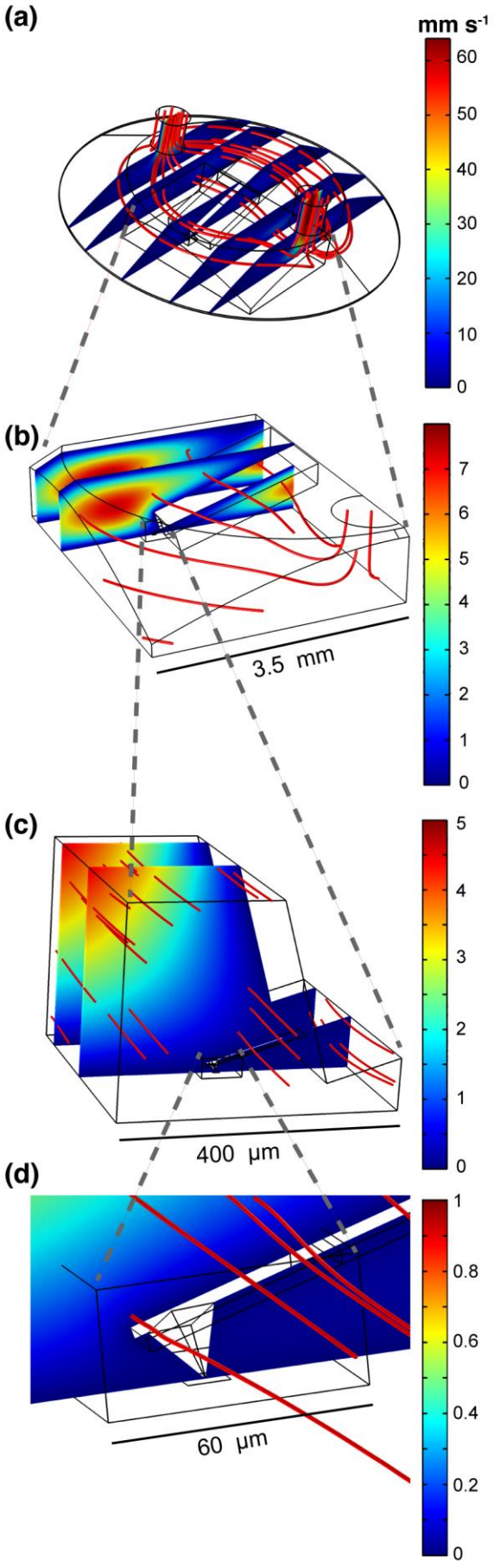
(a)
mm s-1
60
50
40
30
20
10
0
(b)
7
6
5
4
3
2
1
0
3.5 mm
(c)
5
4
3
2
1
0
400 µm
(d)
1
0.8
0.6
0.4
0.2
0
60 µm

Figure 7. Views of the velocity fields within the AFM flow cell at different scales, simulated for a flow rate of 50 µl s^{-1} (increasing magnification from **a** to **d**). Stream lines are shown in red.

Our numerical simulation examined the case where the bottom surface of the fluid cell is mainly formed by a uniformly active area with a $k^{app} = 5 \times 10^{-6}$ m s^{-1}. The bulk solution contained no calcium sulphate (maximum undersaturation). In the ROI, we applied an inert surface boundary condition, based on the results above for the OF model which showed that the processes and conditions in the ROI are controlled essentially by the outer flux. For a flow rate of 50 µl s^{-1}, Figure 8**a, b** clearly shows the formation of a CBL that extends vertically for ≈ 200 µm, and permeates over the entire crystal surface. Over the free part of the crystal, the interfacial concentration is of the order 4 - 5 mM and further increases close to the tip holder reaching 7 mM at the ROI. The plot in Figure 8**c** shows the change of the average concentration in the ROI with flow rate. It can be seen that over the range of interest there is a relatively high interfacial concentration, *i.e.* the reaction is always under mixed transport-surface kinetic control and can never be considered to be purely kinetically controlled (for which the interfacial concentration would be the same as in bulk, with no concentration gradient). Note that over the range of (high) flow rate, from 50 - 100 µl s^{-1}, the interfacial concentration only changes slightly with flow rate (due to the hydrodynamics of the system), which would lead to a more or less constant dissolution rate (step velocity). Without knowledge of the hydrodynamics, one could then, naively, misinterpret data obtained in this situation (2 different flow rates) as being a purely surface–controlled situation, which would be the wrong analysis. This result highlights the danger of simply changing the flow rate until the step velocity remains constant and assuming the reaction must be controlled by surface kinetics as has commonly been done.[35,36,62]

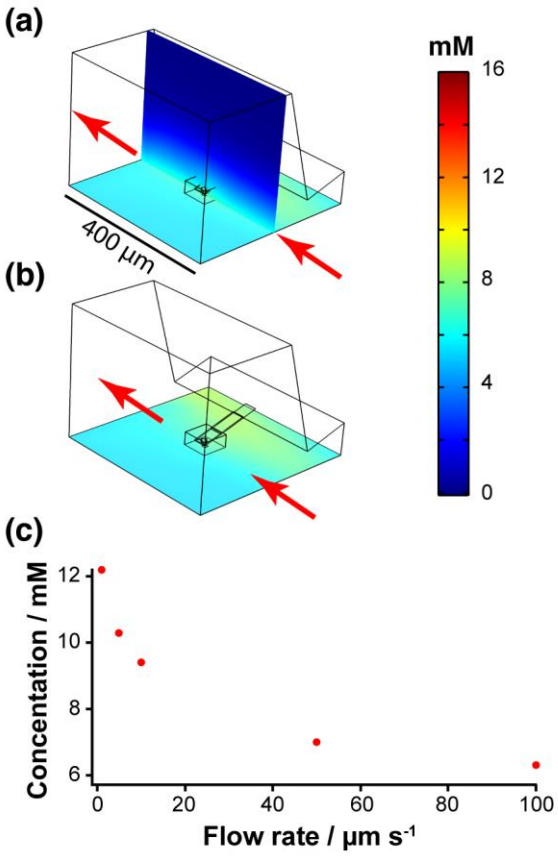

Figure 8. (**a**, **b**) Concentration profiles of Ca^{2+}/SO_4^{2-} at basal crystal surface and perpendicular to the basal surface (near the tip) for $C_b = 0$, $k^{app} = 5 \times 10^{-6}$ m s^{-1} and $V_f = 50$ µl s^{-1}, the red arrows indicate the direction of the solution flow. (**c**) Ca^{2+}/SO_4^{2-} average concentration at the interface in the ROI as a function of flow rate.

In the low flow rate regime, the simulations further demonstrate that the overall reaction tends to a transport-controlled situation, with high interfacial concentrations (approaching saturated values) serving to greatly reduce the dissolution kinetics in the ROI simply due to dissolution processes that occur in the area outside this region.

CONCLUSIONS

The work herein clearly shows that practical AFM fluid cells operating at the range of flow rates defined in the literature offer relatively low interfacial mass transport rates. This is the case even if the "washout time" is high enough to replenish the cell with fresh solution; the "washout" time constant says little about interfacial mass transport rates in such cells. Consequently, if experimental measurements with other techniques (which have higher mass transport rates) show mixed-kinetics for dissolution processes (i.e. with a significant mass transport contribution) one can readily expect that AFM fluid cells will show even more significant mass transport effects. This is the case for gypsum single crystal system considered herein: the hydrodynamics of an AFM fluid cell do not provide sufficiently high mass transport to obtain pure surface kinetic control of crystal dissolution.

A major finding of our study is that step velocities imaged in the AFM ROI are strongly influenced by reactive fluxes from active regions of the crystal outside the ROI. The models we have developed explain why gypsum dissolution rates extracted from AFM step velocities in the literature are orders of magnitude lower than the gross dissolution rates measured by macroscopic techniques. Importantly, we have been able to use our OF model, together with step velocities from etching studies (free from mass transport effects), to successfully predict AFM step velocities in the literature, clearly illustrating how these velocities and associated intrinsic dissolution kinetics are strongly influenced by neighboring dissolution fluxes in adjacent regions of a crystal surface. The issues considered in this paper for crystal dissolution are generally applicable to other dissolution and crystal growth systems and help to explain the 'kinetic gap' that has been evidenced in a number of such studies.[8,35,49,63]

The models developed herein have highlighted quantitatively a number of key issues for AFM dissolution studies. For uniformly distributed steps over a surface, the step velocities are the inverse of the step density in the diffusion-controlled limit, and consequently step densities should be reported as well as velocities. This would provide a check on the kinetic regime. However, in general, the major impact of outer-flux processes on the ROI itself must be accounted for in the measurement of intrinsic rates.

The question then arises as how best to obtain intrinsic rates of crystal growth/dissolution from AFM. Our studies indicate that one needs to know in detail processes occurring outside the ROI and the simplest approach is to define conditions where the flux outside the AFM ROI is zero. A straightforward means of implementing this, as suggested by the results of this paper, our previous work, [58,64-67] and the work of other groups[32,38,43-45] is to investigate micro-crystals on an otherwise inert substrate, or single isolated etch pits on an otherwise inert surface.[58] As we have pointed out in recent studies, this type of configuration is further beneficial in that interfacial mass transport between the surface and bulk solution is extremely efficient, as is well known in electrochemistry with micro/nanoelectrode studies.[68-70] The resulting high transport rates allow investigation of extremely fast dissolution kinetics.[58,66] If studies of larger crystals are mandatory, for practical reasons, then it is important that models are used which account for processes occurring across the entire crystal and not just in the ROI, and the work in this paper provides a roadmap for the analysis of such processes.

AUTHOR INFORMATION

The manuscript was written through contributions of all authors. All authors have given approval to the final version of the manuscript.

ACKNOWLEDGMENT

This work was supported by the European Research council (ERC-2009-AdG247143-QUANTIF). M.A.-V. acknowledges funding from the European Union under a Marie Curie Initial Training Network FP7-PEOPLE-2012-ITN Grant Agreement Number 316630 CAS-IDP. Some of the equipment used in this research was obtained through Birmingham Science City with support from Advantage West Midlands and the European Regional Development Fund.

ABBREVIATIONS

AFM, atomic force microscopy; RD, rotating disk; CFC, channel flow cell; CBL, concentration boundary layer; IE-AFM, integrated electrochemical–atomic force microscopy; SECM-AFM, scanning electrochemical–atomic force microscopy; ROI, region of interest; DIC, differential interference contrast; OCC, open channel cell; US, uniform step; OF, outer flux; MV, molar volume; A_{sd}, distance between steps; A_a, active area; A_i, inactive area, or buffer area; H_b, thickness of concentration boundary layer; D, diffusion coefficient; H_{step}, height of a step; d_{step}, step density; $k_{\mathrm{step}}^{\mathrm{intr}}$, intrinsic dissolution rate constant of a step; k^{app}, apparent dissolution rate constant, average dissolution rate constants for an heterogeneous surface; $k_{\mathrm{surf}}^{\mathrm{intr}}$, intrinsic dissolution rate constant of a surface; k^t, transport rate constant; $J_{\perp}$, inward normal flux of dissolving species; u_{step}, step velocity; t_{diff}, diffusion time; l_p, length of interest, V_{f}, flow rate; C, concentration; C^{sat}, concentration at saturation; C_{b}, bulk concentration; C_{surf}, concentration at the surface; Ω,

saturation; G_{surf}, dissolution rate calculated at geometric surface; G_{surf}^{intr}, dissolution rate at calculated at geometric surface free from mass transport.

REFERENCES

1. Brantley, S. L.; Kibicki, J. D.; White, A. F. *Kinetics of water-rock interaction*; Springer Science: New York, US, 2008.

2. Unwin, P. R.; Macpherson, J. V. New Strategies for Probing Crystal Dissolution Kinetics ate the Microscopic Level. *Chem. Soc. Rev.* **1995**, *24*, 109-119.

3. Macpherson, J. V.; Unwin, P. R. Faraday communications. A New Approach to the Study of Dissolution Kinetics. *J. Chem. Soc., Faraday Trans.* **1993**, *89*, 1883-1884.

4. Unwin, P. R. The Marlow Medal Lecture: Dynamic Electrochemistry as a Quantitative Probe of Interfacial Physicochemical Processes. *J. Chem. Soc., Faraday Trans.* **1998**, *94*, 3183-3195.

5. De Baere, B.; Molins, S.; Mayer, K. U.; François, R. Determination of Mineral Dissolution Regimes Using Flow-Through Time-Resolved Analysis (FT-TRA) and Numerical Simulation. *Chem. Geol.* **2016**, *430*, 1-12.

6. Jones, C. E.; Macpherson, J. V.; Unwin, P. R. In Situ Observation of the Surface Processes Involved in Dissolution from the (010) Surface of Potassium Ferrocyanide Trihydrate in Aqueous Solution Using an Integrated Electrochemical−Atomic Force Microscope. *J. Phys. Chem. B* **2000**, *104*, 2351-2359.

7. Malkin, A. J.; Kuznetsov, Y. G.; Glantz, W.; McPherson, A. Atomic Force Microscopy Studies of Surface Morphology and Growth Kinetics in Thaumatin Crystallization. *J. Phys. Chem.* **1996**, *100*, 11736.

8. Arvidson, R. S.; Ertan, I. E.; Amonette, J. E.; Lüttge, A. Variation in Calcite Dissolution Rates: A Fundamental Problem? *Geochim. Cosmochim. Acta* **2003**, *67*, 1623-1634.

9. Hillner, P. E.; Gratz, A. J.; Manne, S.; Hansma, P. K. Atomic-Scale Imaging of Calcite Growth and Dissolution in Real Time. *Geology* **1992**, *20*, 359-362.

10. Lea, A. S.; Amonette, J. E.; Baer, D. R.; Liang, Y.; Colton, N. G. Microscopic Effects of Carbonate, Manganese, and Strontium Ions on Calcite Dissolution. *Geochim. Cosmochim. Acta* **2001**, *65*, 369-379.

11. Perrin, C. M.; Swift, J. A. Step Kinetics on Monosodium Urate Monohydrate Single Crystal Surfaces: An In Situ AFM Study. *CrystEngComm* **2012**, *14*, 1709-1715.

12. Pinto, A. J.; Ruiz-Agudo, E.; Putnis, C. V.; Putnis, A.; Jimenez, A.; Prieto, M. AFM Study of the Epitaxial Growth of Brushite on Gypsum Cleavage Surfaces. *Am. Mineral.* **2010**, *95*, 1747-1757.

13. Ruiz-Agudo, E.; Putnis, C. V. Direct Observations of Mineral-Fluid Reactions using Atomic Force Microscopy: The Specific Example of Calcite. *Mineral. Mag.* **2012**, *76*, 227-253.

14. Xu, M.; Higgins, S. R. Effects of Magnesium Ions on Near-Equilibrium Calcite Dissolution: Step Kinetics and Morphology. *Geochim. Cosmochim. Acta* **2011**, *75*, 719-733.

15. Kuwahara, Y.; Makio, M. In Situ AFM Study on Barite (0 0 1) Surface Dissolution in NaCl Solutions at 30 °C. *Appl. Geochem.* **2014**, *51*, 246-254.

16. Burgos-Cara, A.; Putnis, C. V.; Rodriguez-Navarro, C.; Ruiz-Agudo, E. Hydration Effects on Gypsum Dissolution Revealed by In Situ Nanoscale Atomic Force Microscopy Observations. *Geochim. Cosmochim. Acta* **2016**, *179*, 110-122.

17. Bracco, J. N.; Gooijer, Y.; Higgins, S. R. Growth Kinetics of Step Edges on Celestite (0 0 1) Surfaces as a Function of Temperature, Saturation State, Ionic Strength, and Aqueous Strontium:Sulfate Ratio: An In-Situ Atomic Force Microscopy Study. *Geochim. Cosmochim. Acta* **2016**, *175*, 222-238.

18. Klasa, J.; Ruiz-Agudo, E.; Wang, L. J.; Putnis, C. V.; Valsami-Jones, E.; Menneken, M.; Putnis, A. An Atomic Force Microscopy Study of the Dissolution of Calcite in the Presence of Phosphate Ions. *Geochim. Cosmochim. Acta* **2013**, *117*, 115-128.

19. Dove, P. M.; Platt, F. M. Compatible Real-Time Rates of Mineral Dissolution by Atomic Force Microscopy (AFM). *Chem. Geol.* **1996**, *127*, 331-338.

20. Jordan, G.; Rammensee, W. Dissolution Rates of Calcite (104) Obtained by Scanning Force Microscopy: Microtopography-Based Dissolution Kinetics on Surfaces with Anisotropic Step Velocities. *Geochim. Cosmochim. Acta* **1998**, *62*, 941-947.

21. McPherson, A.; Malkin, A. J.; Kuznetsov, Y. G. Atomic Force Microscopy in the Study of Macromolecular Crystal Growth. *Annu. Rev. Biophys. Biomol. Struct.* **2000**, *29*, 361-410.

22. Tang, R.; Nancollas, G. H.; Orme, C. A. Mechanism of Dissolution of Sparingly Soluble Electrolytes. *J. Am. Chem. Soc.* **2001**, *123*, 5437-5443.

23. Land, T. A.; De Yoreo, J. J.; Lee, J. D. An In-Situ AFM Investigation of Canavalin Crystallization Kinetics. *Surf. Sci.* **1997**, *384*, 136-155.

24. Hillier, A. C.; Ward, M. D. Atomic Force Microscopy of the Electrochemical Nucleation and Growth of Molecular Crystals. *Science* **1994**, *263*, 1261-1264.

25. Larsen, K.; Bechgaard, K.; Stipp, S. L. S. The Effect of the Ca_2^+ to Activity Ratio on Spiral Growth at the Calcite Surface. *Geochim. Cosmochim. Acta* **2010**, *74*, 2099-2109.

26. Macpherson, J. V.; Unwin, P. R.; Hillier, A. C.; Bard, A. J. In-Situ Imaging of Ionic Crystal Dissolution Using an Integrated Electrochemical/AFM Probe. *J. Am. Chem. Soc.* **1996**, *118*, 6445-6452.

27. Jones, C. E.; Unwin, P. R.; Macpherson, J. V. In Situ Observation of the Surface Processes Involved in Dissolution from the Cleavage Surface of Calcite in Aqueous Solution

Using Combined Scanning Electrochemical–Atomic Force Microscopy (SECM-AFM). *ChemPhysChem* **2003**, *4*, 139-146.

28. Jones, C. E.; Macpherson, J. V.; Barber, Z. H.; Somekh, R. E.; Unwin, P. R. Simultaneous Topographical and Amperometric Imaging of Surfaces in Air: Towards a Combined Scanning Force-Scanning Electrochemical Microscope (SF-SECM). *Electrochem. Commun.* **1999**, *1*, 55-60.

29. Izquierdo, J.; Fernández-Pérez, B. M.; Eifert, A.; Souto, R. M.; Kranz, C. Simultaneous Atomic Force-Scanning Electrochemical Microscopy (AFM-SECM) Imaging of copper dissolution *Journal* **2015**, DOI: 10.1016/j.electacta.2015.12.160.

30. Teng, H. H. Controls by Saturation State on Etch Pit Formation during Calcite Dissolution. *Geochim. Cosmochim. Acta* **2004**, *68*, 253-262.

31. Cama, J.; Zhang, L.; Soler, J. M.; Giudici, G. D.; Arvidson, R. S.; Lüttge, A. Fluorite Dissolution at Acidic pH: In Situ AFM and Ex Situ VSI Experiments and Monte Carlo Simulations. *Geochim. Cosmochim. Acta* **2010**, *74*, 4298-4311.

32. Hall, C.; Cullen, D. C. Scanning Force Microscopy of Gypsum Dissolution and Crystal Growth. *AIChE J.* **1996**, *42*, 232-238.

33. Van Driessche, A. E. S.; Garci a-Ruiz, J. M.; Delgado-Lo pez, J. M.; Sazaki, G. In Situ Observation of Step Dynamics on Gypsum Crystals. *Cryst. Growth Des.* **2010**, *10*, 645-682.

34. Ruiz-Agudo, E.; Putnis, C.; Jiménez-López, C.; Rodriguez-Navarro, C. An Atomic Force Microscopy Study of Calcite Dissolution in Saline Solutions: The Role of Magnesium Ions. *Geochim. Cosmochim. Acta* **2009**, *73*, 3201-3217.

35. Shiraki, R.; Rock, P. A.; Casey, W. H. Dissolution Kinetics of Calcite in 0.1 M NaCl Solution at Room Temperature: An Atomic Force Microscopic (AFM) Study. *Aquat. Geochem.* **2000**, *6*, 87-108.

36. Liang, Y.; Baer, D. R. Anisotropic Dissolution at the $CaCO_3$ (10(1)over-bar4)-Water Interface. *Surf. Sci.* **1997**, *373*, 275-287.

37. De Giudici, G. Surface Control vs. Diffusion Control during Calcite Dissolution: Dependence of Step-Edge Velocity upon Solution pH. *Am. Mineral.* **2002**, *87*, 1279-1285.

38. Gasperino, D.; Yeckel, A.; Olmsted, B. K.; Ward, M. D.; Derby, J. J. Mass Transfer Limitations at Crystallizing Interfaces in an Atomic Force Microscopy Fluid Cell: A Finite Element Analysis. *Langmuir* **2006**, *22*, 6578-6586.

39. Klimchouk, A. Sulphate Rocks as an Arena for Karst Development. *Int. J. Speleol.* **1996**, *25*, 9-20.

40. Kovler, K. Setting and Hardening of Gypsum-Portland Cement-Silica Fume Blends, Part 1: Temperature and Setting Expansion. *Cem. Concr. Res* **1998**, *28*, 423-437.

41. Colombani, J. Measurement of the Pure Dissolution Rate Constant of a Mineral in Water. *Geochim. Cosmochim. Acta* **2008**, *72*, 5634-5640.

42. Bosbach, D.; Hochella Jr, M. F. Gypsum Growth in the Presence of Growth Inhibitors: a Scanning Force Microscopy Study. *Chem. Geol.* **1996**, *132*, 227-236.

43. Bosbach, D.; Rammensee, W. In Situ Investigation of Growth and Dissolution on the (010) Surface of Gypsum by Scanning Force Microscopy. *Geochim. Cosmochim. Acta* **1994**, *58*, 843-849.

44. Fan, C.; Teng, H. H. Surface Behavior of Gypsum during Dissolution. *Chem. Geol.* **2007**, *245*, 242-253.

45. Pachon-Rodriguez, E. A.; Piednoir, A.; Colombani, J. Pressure Solution at the Molecular Scale. *Phys. Rev. Lett.* **2011**, *107*, 146102-146104.

46. Duckworth, O. W.; Martin, S. T. Dissolution Rates and Pit Morphologies of Rhombohedral Carbonate Minerals. *Am. Mineral.* **2004**, *89*, 554.

47. Burt, D. P.; Wilson, N. R.; Janus, U.; Macpherson, J. V.; Unwin, P. R. In-Situ Atomic Force Microscopy (AFM) Imaging: Influence of AFM Probe Geometry on Diffusion to Microscopic Surfaces. *Langmuir* **2008**, *24*, 12867-12876.

48. *CRC Handbook of Chemistry and Physics*, 90th Edition (Internet Version 2010) ed.; CRC Press: Florida, US, 2010.

49. Mbogoro, M. M.; Snowden, M. E.; Edwards, M. A.; Peruffo, M.; Unwin, P. R. Intrinsic Kinetics of Gypsum and Calcium Sulfate Anhydrite Dissolution: Surface Selective Studies under Hydrodynamic Control and the Effect of Additives. *J. Phys. Chem. C* **2011**, *115*, 10147-10154.

50. Schecher, W. D. *A Chemical Equilibrium Modelling System*; Hallowell: Maine, US, 2003.

51. Brett, C. M. A.; Brett, A. M. O. *Electrochemistry: Principles, Methods, and Applications*; Oxford University Press: Oxford, UK, 1993; Vol. 14, p 978-984.

52. Liu, S.-T.; Nancollas, G. H. The Kinetics of Dissolution of Calcium Sulfate Dihydrate. *J. Inorg. Nucl. Chem.* **1971**, *33*, 2311-2316.

53. Christoffersen, J.; Christoffersen, M. R. The Kinetics of Dissolution of Calcium Sulphate Dihydrate in Water. *J. Cryst. Growth* **1976**, *35*, 79-88.

54. Carmichael, R. S. *Practical handbook of physical properties of rocks and minerals* CRC Press: Boca Raton, Fla, 1989.

55. González, B.; Calvar, N.; Gómez, E.; Domínguez, Á. Density, Dynamic Viscosity, and Derived Properties of Binary Mixtures of Methanol or Ethanol with Water, Ethyl Acetate, and Methyl Acetate at T = (293.15, 298.15, and 303.15) K. *J. Chem. Thermodynamics* **2007**, *39*, 1578-1588.

56. Jeschke, A. A.; Vosbeck, K.; Dreybrodt, W. Surface Controlled Dissolution Rates of Gypsum in Aqueous Solutions Exhibit Nonlinear Dissolution Kinetics. *Geochim. Cosmochim. Acta* **2001**, *65*, 27-34.

57. Raines, M. A.; Dewers, T. A. Mixed Transport/Reaction Control of Gypsum Dissolution Kinetics in Aqueous Solutions and Initiation of Gypsum Karst. *Chem. Geol.* **1997**, *140*, 29-48.

58. Peruffo, M.; Mbogoro, M. M.; Edwards, M. A.; Unwin, P. R. Holistic Approach to Dissolution Kinetics: Linking Direction-Specific Microscopic Fluxes, Local Mass Transport Effects and Global Macroscopic Rates from Gypsum Etch Pit Analysis. *Phys. Chem. Chem. Phys.* **2013**, *15*, 1956-1965.

59. Zhang, J.; Nancollas, G. H. Kink Densities along a Crystal Surface Step at Low Temperatures and under Nonequilibrium Conditions. *J. Cryst. Growth* **1990**, *106*, 181-190.

60. Sangwal, K. *Etching of Crystals: Theory, experiment, and application*; North-Holland Amsterdam: Amsterdam, NL, 1987; Vol. 497.

61. MacInnis, I. N.; Brantley, S. L. The Role of Dislocations and Surface Morphology in Calcite Dissolution. *Geochim. Cosmochim. Acta* **1992**, *56*, 1113-1126.

62. Higgins, S. R.; Jordan, G.; Eggleston, C. M. Dissolution Kinetics of Magnesite in Acidic Aqueous Solution: a Hydrothermal Atomic Force Microscopy Study Assessing Step Kinetics and Dissolution Flux. *Geochim. Cosmochim. Acta* **2002**, *66*, 3201-3210.

63. Sjöberg, E. L.; Rickard, D. T. Calcite Dissolution Kinetics - Surface Speciation and the Origin of the Variable pH-Dependence *Chem. Geol.* **1984**, *42*, 119-136.

64. Dobson, P. S.; Bindley, L. A.; Macpherson, J. V.; Unwin, P. R. Modes of Action of a Weak Acid Modifier of Calcite Growth. *ChemPhysChem* **2006**, *7*, 1019-1021.

65. Dobson, P. S.; Bindley, L. A.; Macpherson, J. V.; Unwin, P. R. Atomic Force Microscopy Investigation of the Mechanism of Calcite Microcrystal Growth under Kitano Conditions. *Langmuir* **2005**, *21*, 1255-1260.

66. Perry, A. R.; Peruffo, M.; Unwin, P. R. Quantitative Plane-Resolved Crystal Growth and Dissolution Kinetics by Coupling In Situ Optical Microscopy and Diffusion Models: The Case of Salicylic Acid in Aqueous Solution. *Cryst. Growth Des.* **2013**.

67. Perry, A. R.; Lazenby, R. A.; Adobes-Vidal, M.; Peruffo, M.; McKelvey, K.; Snowden, M. E.; Unwin, P. R. Hopping Intermittent Contact-Scanning Electrochemical Microscopy (HIC-SECM) as a New Local Dissolution Kinetic Probe: Application to Salicylic Acid Dissolution in Aqueous Solution. *CrystEngComm* **2015**, *17*, 7835-7843.

68. Heinze, J. Ultramicroelectrodes in Electrochemistry. *Angew. Chem., Int. Ed. Engl.* **1993**, *32*, 1268-1288.

69. Forster, R.; Keyes, T. In *Handbook of Electrochemistry*; Elsevier: Oxford, UK, 2006, pp 155-186.

70. Cox, J. T.; Zhang, B. Nanoelectrodes: Recent Advances and New Directions. *Annu. Rev. Anal. Chem.* **2012**, *5*, 253-272.

TABLE OF CONTENT IMAGE